Lin et al., https://doi.org/10.1083/jcb.201606092

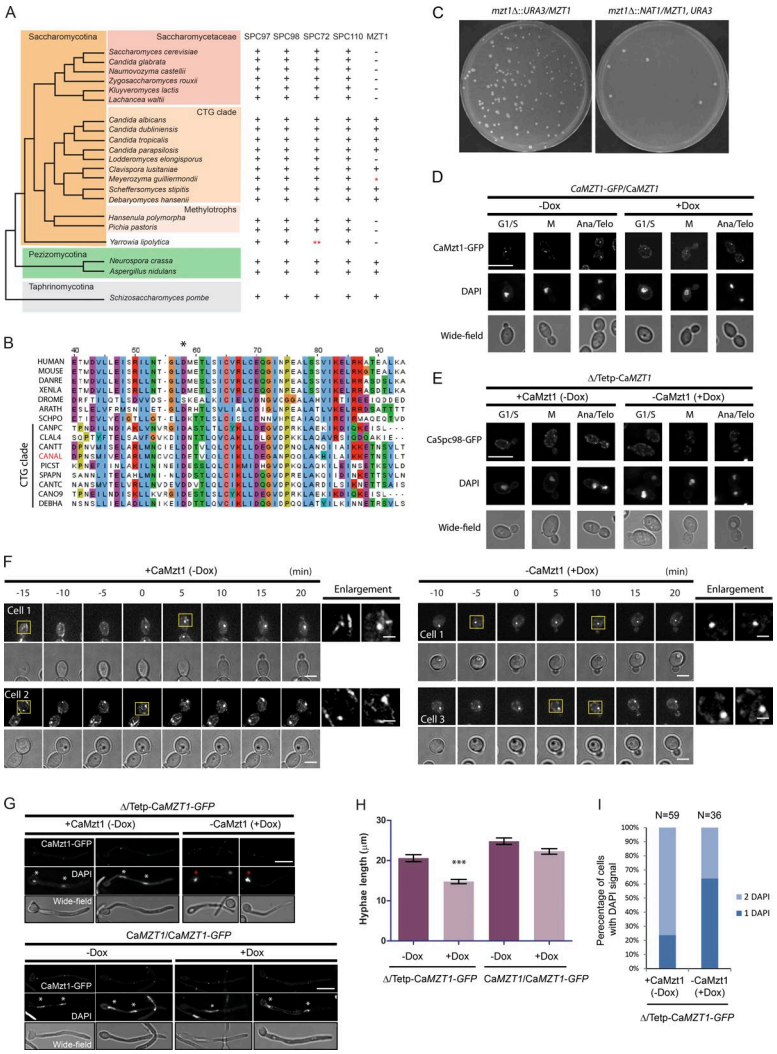

Figure S1. ***CaMZT1* is an essential gene that promotes binding of the Caγ-TuSC to SPBs.** (A) The species cladogram and the presence of γ-TuSC, γ-TuCRs, and *MZT1* homologous genes. Homologous genes were identified by reciprocal BLAST, using queries from *S. cerevisiae*, *S. pombe*, and related species. The species tree is adapted from previous work (Hanson et al., 2014) and shows the approximate phylogenetic relationship of the species. *SPC72* and *SPC110* homologues are evolving rapidly and can be difficult to identify (*SPC72* of *Yarrowia lipolytica*, marked with double red asterisks). The presence of *MZT1* in *Meyerozyma guilliermondii* is unclear because of sequencing gaps (therefore marked with single red asterisk). *MZT1* has been lost from the Saccharomycetaceae and probably independently from the Methylotrophs. The official ORF names and additional annotations are shown in Table S1. (B) Sequence alignment of putative *MZT1* of Saccharomycotina species and Mzt1/MOZART1 orthologues of canonical model organisms including *S. pombe*, Arabidopsis, and human. Only the conserved core region (from residue position 40 to 94 of the aligned sequences) is shown. Residues are marked according to the Clustal X color scheme. The asterisk marks D22 of CaMzt1 that was mutated to alanine in the mutant CaMzt1^{D22A}. (C) *MZT1* appears to be essential in *C. albicans*. *MZT1/MZT1* and *mzt1Δ::NAT1/MZT1* cells were subjected to a round of *MZT1* gene disruption using a *URA3* disruption cassette. *mzt1Δ::URA3/MZT1* cells were obtained with high frequency as shown by colony PCR of transformants. In contrast, only a very small number of URA-positive colonies were obtained in case of *mzt1Δ::NAT1/MZT1*. Analysis of the transformants by PCR showed that they were still *mzt1Δ::NAT1/MZT1*. Thus, in these cells, *URA3* integrated into a locus other than *MZT1*. (D) The localization of CaMzt1-GFP at SPBs was not perturbed in wild-type cells upon Dox (+Dox) treatment. Bar, 10 µm. Related to Fig. 1 A. (E) CaSpc98-GFP was delocalized from SPBs after depletion of CaMzt1 upon Dox treatment. *Δ/Tetp-CaMZT1 CaSPC98-GFP/CaSPC98* cells were grown without and with Dox. Addition of Dox repressed Tetp-*CaMZT1* expression and the dot-like CaSpc98-GFP signal at SPBs was reduced. Bar, 10 µm. Related to Fig. 1 B. (F) Time-lapse of *Δ/Tetp-CaMZT1 CaTUB1-GFP* cells with and without Dox. Time 0 was set as the budding onset. Bars, 5 µm. Enlargements of boxed areas (yellow boxes were enlarged) with free MTs are shown (bars, 2 µm). Cell 1 and Cell 2 (+CaMzt1; left panel) and Cell 1 (−CaMzt1; right panel) correspond to the cells shown in Fig. 1 C. Note that for Cell 2 (+CaMzt1), frames 25 and 30 s are not depicted; for Cell 1 (−CaMzt1), frames 25–65 s are not depicted. Related to Fig. 1 C. (G) Serum-induced hyphal growth was reduced in CaMzt1-depleted cells. *Δ/Tetp-CaMZT1-GFP* and *CaMZT1/CaMZT1-GFP* cells were grown with and without Dox. Addition of serum for 2 h induced hyphae formation. *Δ/Tetp-CaMZT1-GFP* cells in the presence of Dox (−CaMzt1) had only one DAPI staining region in the basal cell (red asterisks). All other cell types had at least one DAPI staining region in the hyphae (white asterisks). Bars, 10 µm. (H) Hyphae length from cells in G was measured from the hyphae tip to the stem neck at the basal cell. n = 160–190 for the number of cells measured in each samples. ***, $P < 0.001$. Error bars represent SEM. (I) Percentage of cells showing one DAPI or two DAPI signals in *Δ/Tetp-CaMZT1-GFP* cells treated with and without Dox. n = 59 and 36 for the number of counted cells in a single experiment without Dox (+CaMzt1) and with Dox (−CaMzt1), respectively. Ana/Telo, anaphase/telophase; M, metaphase.

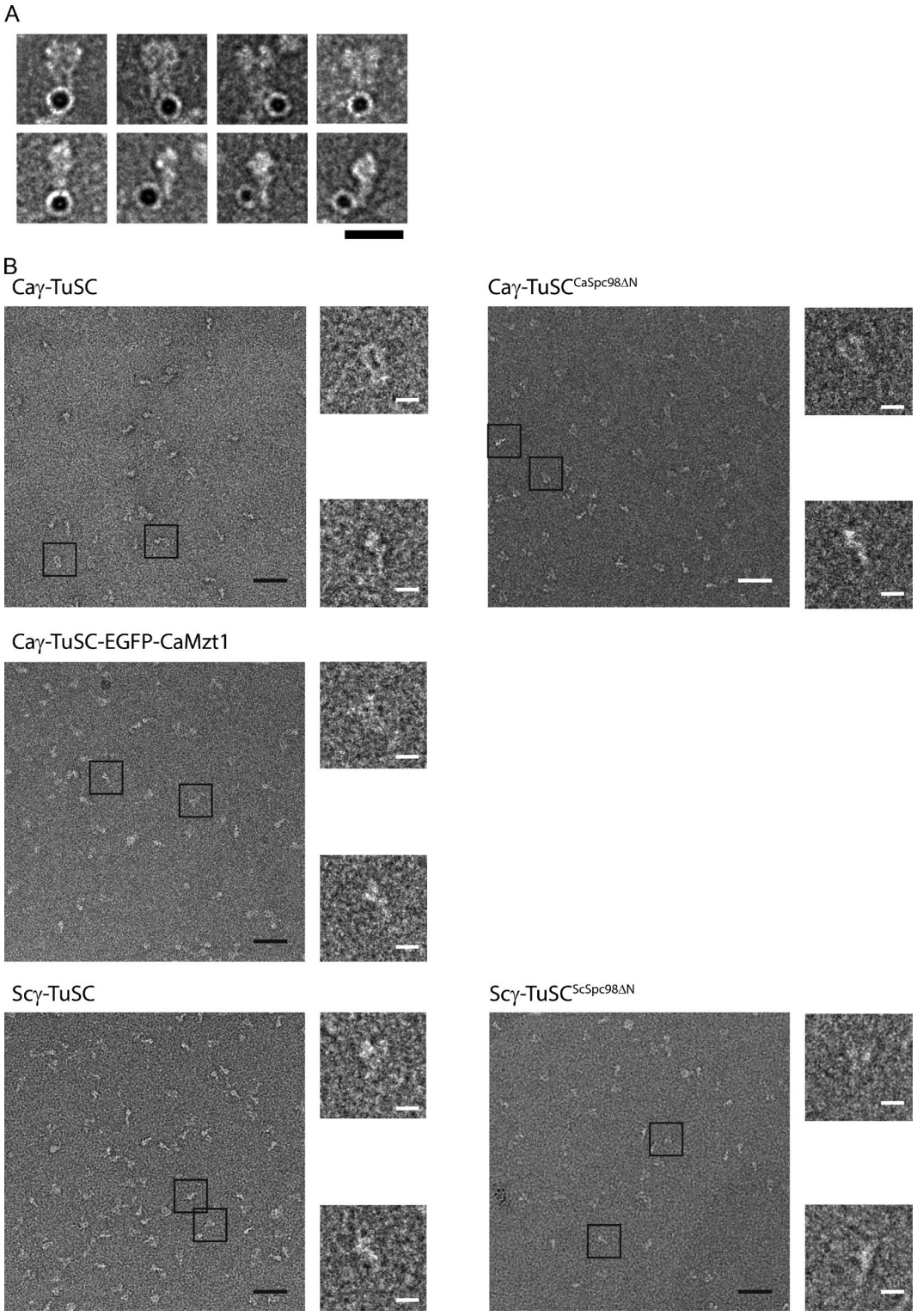

Figure S2. **Negative-stained EM of γ-TuSC particles.** (A) The N-terminal domain of Spc97/Spc98 is located at the base of V/Y-shaped structure of Caγ-TuSC. Caγ-TuSC with 6xHis tag at the N terminus of CaSpc97 and CaSpc98 was labeled with Ni-NTA-Nanogold (5 nm) and subjected to negative staining and EM analysis. Bar, 10 nm. Related to Fig. 2 B. (B) Representative EM micrographs of Caγ-TuSC, Caγ-TuSC$^{CaSpc98\Delta N}$, Caγ-TuSC-EGFP-CaMzt1, Scγ-TuSC, and Scγ-TuSC$^{ScSpc98\Delta N}$. Boxed particles were used in classification and averaging. Bars: (black) 100 nm; (white) 10 nm. Related to Fig. 2 B and Fig. 4, A and B.

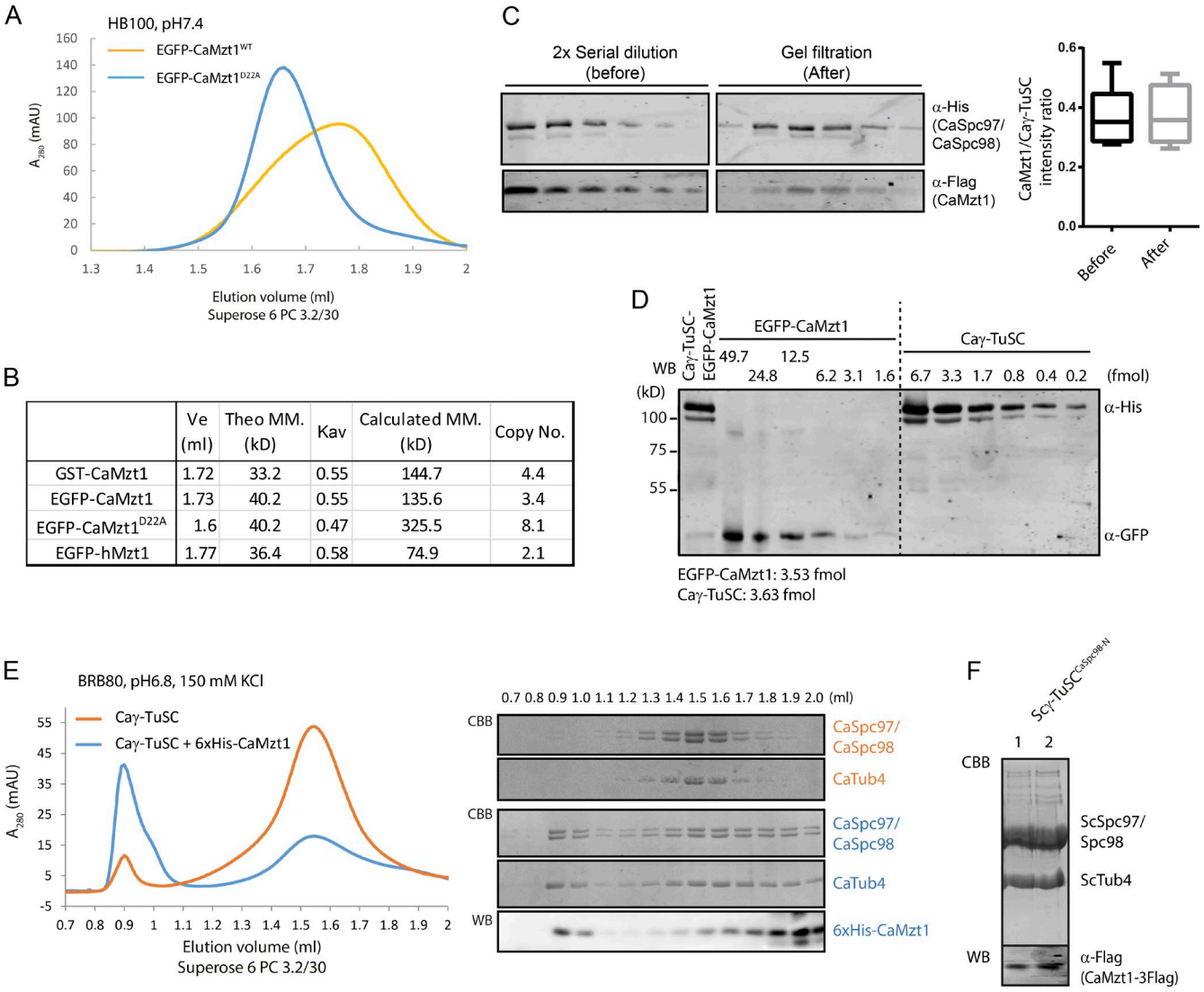

	Ve (ml)	Theo MM. (kD)	Kav	Calculated MM. (kD)	Copy No.
GST-CaMzt1	1.72	33.2	0.55	144.7	4.4
EGFP-CaMzt1	1.73	40.2	0.55	135.6	3.4
EGFP-CaMzt1^{D22A}	1.6	40.2	0.47	325.5	8.1
EGFP-hMzt1	1.77	36.4	0.58	74.9	2.1

Figure S3. **CaMzt1 forms oligomers but stably interacts with Cγ-TuSC in an equal molar ratio.** (A) The gel-filtration profiles of recombinant EGFP-CaMzt1 suggest that it forms oligomers ranging from trimer to tetramer. CaMzt1 with a mutation in the conserved D22 (CaMzt1^{D22A}) residue (Fig. S1 B) that results in a conditional lethal phenotype in *S. pombe* shifted the elution profile to earlier fractions, suggesting the oligomeric status or overall conformation of CaMzt1 was altered. Related to Fig. 3 C. (B) Summary of the deduced oligomerization level of CaMzt1, CaMzt1^{D22A}, and hMzt1 based on gel-filtration analysis. The elution volume (Ve) of each protein peak was used to calculate the molecular mass (MM) based on the calibration curve. The calculated molecular mass was then divided by the theoretical (Theo) molecular mass of each protein, resulting in the copy number. The following protein markers were used to calibrate the gel-filtration column Superose 6 PC 3.2/30: thyroglobulin (667 kD), ferritin (440 kD), aldolase (158 kD), conalbumin (75 kD), and ovalbumin (44 kD). Kav, partition coefficient. Related to Fig. 3 C. (C) To test the integrity of Cγ-TuSC–CaMzt1 complex, Cγ-TuSC–CaMzt1, before and after ion exchange and gel filtration, was analyzed with SDS-PAGE and visualized by Western blotting for 3Flag-tagged CaMzt1 and 6His-tagged CaSpc97 and CaSpc98. Signal intensities were quantified and transformed into the CaMzt1/Cγ-TuSC ratio. $n = 4$ for the number of quantification. Related to Fig. 3, A and B. (D) Quantification of Cγ-TuSC–CaMzt1 molecular ratio. Cγ-TuSC–EGFP–CaMzt1 complex was separated by SDS-PAGE and analyzed by fluorescent Western blotting (WB) together with samples of serial diluted EGFP-CaMzt1 and Cγ-TuSC. Protein concentration and loading amount were estimated by Nanodrop at 280-nm absorbance and calculated according to protein molecular mass and extinction coefficient. Related to Fig. 4 A. (E) 6xHis-CaMzt1 promoted oligomerization of Cγ-TuSC in BRB80, 150 mM KCl. Experiment was performed as described in Fig. 3 F. Related to Fig. 3 F. The control Cγ-TuSC only (150 mM KCl) is the same as shown in Fig. 2 E. (F) CaMzt1-3Flag was stably associated with Scγ-TuSC$^{CaSpc98\text{-}N}$ during ion-exchange chromatography. Two fractions (1 and 2) corresponding to the peak eluted at ~400 mM NaCl were analyzed with SDS-PAGE and visualized with CBB staining. CaMzt1-3Flag was detected with antibody against Flag-tag. Related to Fig. 4 D. mAU, milli-absorbance unit.

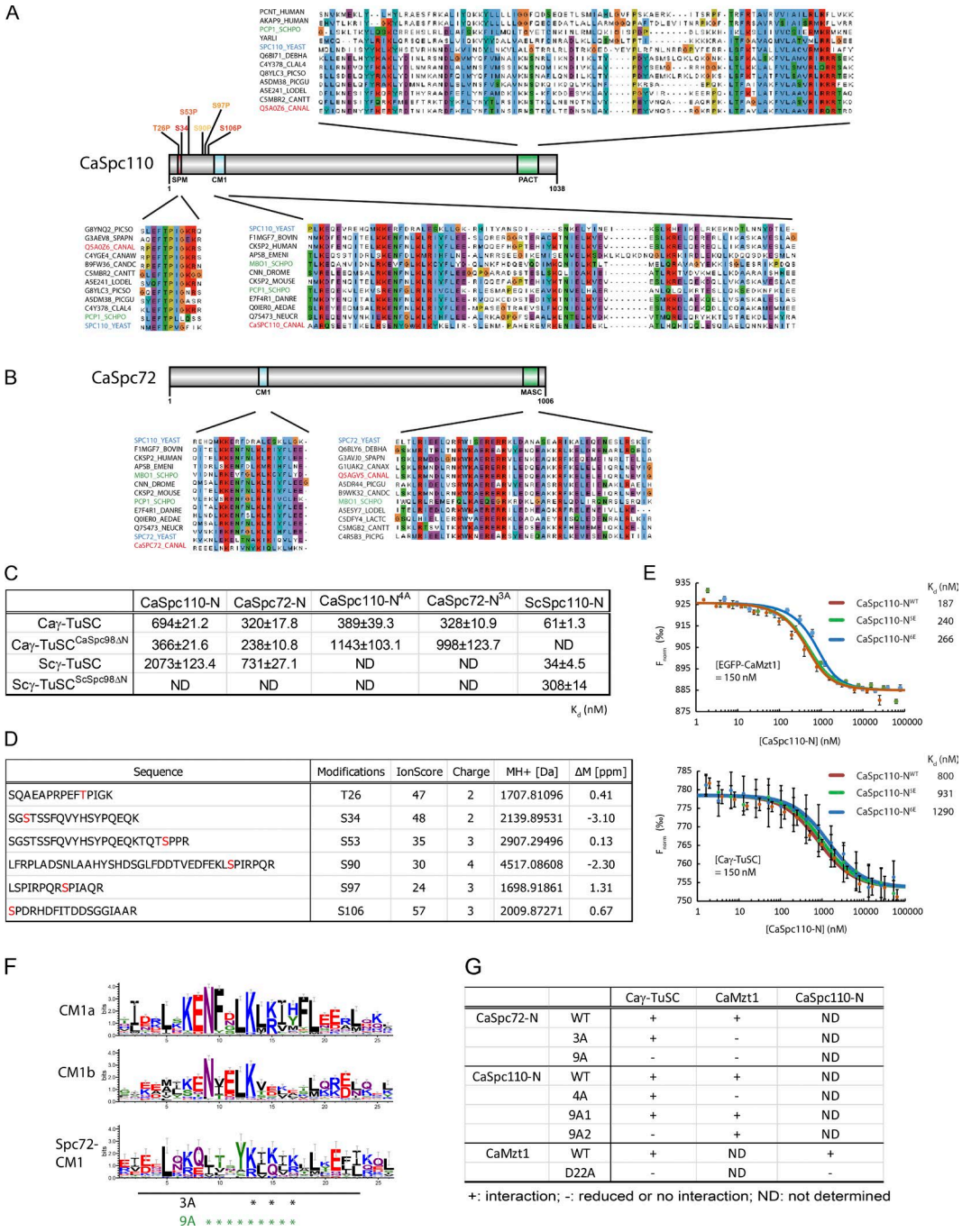

C

	CaSpc110-N	CaSpc72-N	CaSpc110-N^{4A}	CaSpc72-N^{3A}	ScSpc110-N
Caγ-TuSC	694±21.2	320±17.8	389±39.3	328±10.9	61±1.3
Caγ-TuSC$^{CaSpc98\Delta N}$	366±21.6	238±10.8	1143±103.1	998±123.7	ND
Scγ-TuSC	2073±123.4	731±27.1	ND	ND	34±4.5
Scγ-TuSC$^{ScSpc98\Delta N}$	ND	ND	ND	ND	308±14

K_d (nM)

D

Sequence	Modifications	IonScore	Charge	MH+ [Da]	ΔM [ppm]
SQAEAPRPEFTPIGK	T26	47	2	1707.81096	0.41
SGSTSSFQVYHSYPQEQK	S34	48	2	2139.89531	-3.10
SGSTSSFQVYHSYPQEQKTQTSPPR	S53	35	3	2907.29496	0.13
LFRPLADSNLAAHYSHDSGLFDDTVEDFEKLSPIRPQR	S90	30	4	4517.08608	-2.30
LSPIRPQRSPIAQR	S97	24	3	1698.91861	1.31
SPDRHDFITDDSGGIAAR	S106	57	3	2009.87271	0.67

E

G

		Caγ-TuSC	CaMzt1	CaSpc110-N
CaSpc72-N	WT	+	+	ND
	3A	+	-	ND
	9A	-	-	ND
CaSpc110-N	WT	+	+	ND
	4A	+	-	ND
	9A1	+	+	ND
	9A2	-	+	ND
CaMzt1	WT	+	ND	+
	D22A	-	ND	-

+: interaction; -: reduced or no interaction; ND: not determined

Figure S4. **Different requirements for residues within the CM1 for the binding to CaMzt1 and γ-TuSC.** (A) Motif organization of CaSpc110. The conserved N-terminal SPM and CM1 elements and C-terminal PACT domain are shown. The sequences of each motif from homologues of selected species were aligned with MAFFT algorithm. The representative model organisms *S. cerevisiae*, *C. albicans*, and *S. pombe* are marked in blue, red, and green, respectively. Related to Fig. 5 B. (B) Motif organization of CaSpc72. The conserved N-terminal short CM1 element and C-terminal MASC domain are shown. The sequences of each motif from homologues of selected species were aligned with MAFFT algorithm. The representative model organisms *S. cerevisiae*, *C. albicans*, and *S. pombe* are marked in blue, red, and green, respectively. (C) Summary of binding affinity measurement among various γ-TuSCs and receptors with microscale thermophoresis. K_d ± SD; n = 3 for the number of independent measurements. (D) CaSpc110-N overexpressed in insect cells was phosphorylated within the linker between the SPM and CM1 motifs. Phosphorylation sites were identified with mass spectrometry in the purified CaSpc110-N from insect cells. The conserved phosphorylation site within SPM was also identified. The font color of phosphorylation sites shown in A represents the relative level of frequency of identification. Whereas red font represents the highest frequency, yellow font represents lowest frequency. (E) The phospho-mimicking CaSpc110-N^{5E} or CaSpc110-N^{6E} mutant proteins did not significantly affect binding to EGFP-CaMzt1 or Caγ-TuSC as measured by MST analysis. Four records from two independent sample preparations were collected, and the averaged values were subjected to binding curve fitting with NanoTemper software. Error bars represent SD. The data shown are from a single representative measurement out of three independent measurements. Experiment was performed as described in Fig. 4 E. Related to Figs. 4 E and 5 D. (F) Weblogo presentation of the two conserved subregions of CM1. CM1 sequences of all γ-TuCRs featuring CM1 element were aligned. The nonconserved region was used as a boundary to divide the CM1 alignment into two regions, CM1a and CM1b. The three black asterisks highlight the mutated charged residues in CaSpc72-N^{3A}. The consecutive nine mutation sites of the CaSpc72-N^{9A} are marked with green asterisks. Related to B. (G) Summary of effect of CaSpc110-N and CaSpc72-N mutations on the binding to CaMzt1 and Caγ-TuSC.

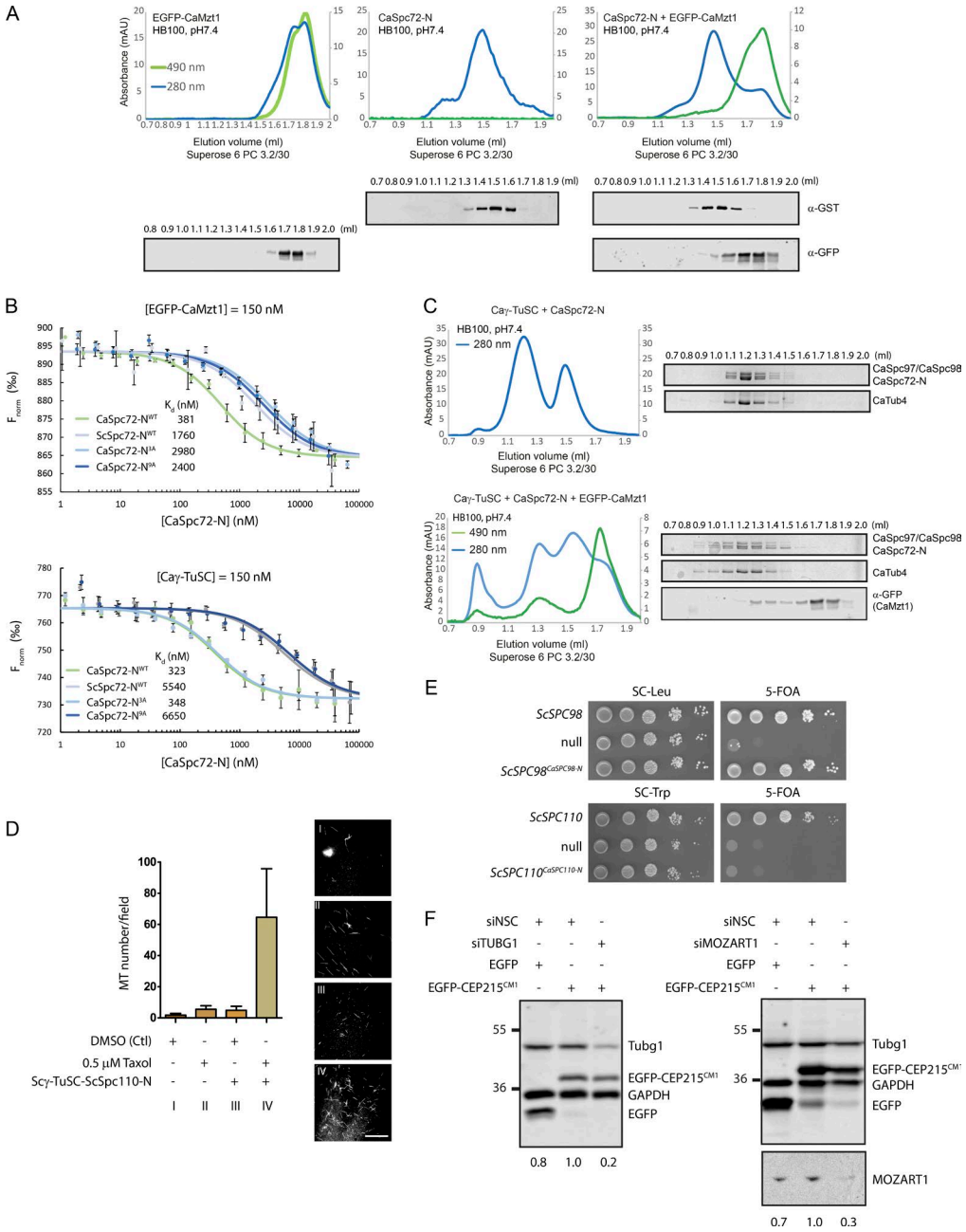

Figure S5. **Interaction among CaSpc72-N, Caγ-TuSC, and CaMzt1, plus additional related data.** (A) Analysis of complex formation of recombinant and purified EGFP-CaMzt1, CaSpc72-N, and CaSpc72-N EGFP-CaMzt1 by Superose 6 PC3.2/30 gel filtration. The elution fractions were analyzed by SDS-PAGE and visualized by Western blotting with anti-GST (for CaSpc72-N) and anti-GFP (for CaMzt1). Related to Fig. 5 A. (B) MST measurement of the binding of EGFP-CaMzt1 and Caγ-TuSC to CaSpc72-N variants. The interaction between EGFP-CaMzt1^{WT} and CaSpc72-N was abolished when three point mutations (3A) were introduced into CM1 of CaSpc72-N. EGFP-CaMzt1 was kept at constant concentration 150 nM, and 16 titration points ranging from ∼1 nM to ∼50 μM were prepared from a serial dilution of GST–CaSpc72-N. Four records from two independent sample preparations were collected, and the averaged values were subjected to binding curve fitting with NanoTemper software. Error bars represent SD. The data shown are from a single representative experiment out of three independent experiments. Related to Figs. 4 E and 5 D. (C) CaMzt1 and CaSpc72-N are both required to promote Caγ-TuSC oligomerization under oligomer-disfavored conditions. Independently purified CaMzt1 and CaSpc72-N were incubated with Caγ-TuSC in HB100 buffer, pH 7.4, and analyzed by gel filtration. Absorbance at 490 nm was monitored for the migration of EGFP-CaMzt1. Fractions were analyzed by SDS-PAGE and visualized by CBB staining. EGFP-CaMzt1 was detected by immunoblotting. Related to Fig. 6, A and B. (D) Effect of taxol on MT stabilization in in vitro MT nucleation assay. (left) Statistical result of in vitro MT nucleation assay. For each sample (I–IV), MT numbers were counted in eight random fields. Error bars show SD. (right) Maximum projected images of the eight acquired fields for experiments I–IV. Bar, 50 μm. Related to Fig. 6 F. (E) *ScSPC98*$^{CaSPC98\text{-}N}$ complemented the essential function of *ScSPC98*, whereas *ScSPC110*$^{CaSPC110\text{-}N}$ failed to complement *ScSPC110*. Growth of 10-fold serial dilutions of *SPC98* and *SPC110* shuffle strains with *CEN*-plasmid encoding *ScSPC98* and *ScSPC110* wild type or mutant, respectively. Growth was tested either on synthetic complete (SC) plates containing 5-fluoroorotic acid (5-FOA) or SC dropout plates at 23°C. Related to Fig. 6 G. (F) siRNA knockdown of MOZART1 and γ-tubulin and *EGFP-CEP215*^{CM1} overexpression in U2OS cells. 1% total cell lysates was boiled with sample buffer and then loaded on 10% SDS gel for SDS-PAGE and Western blot analysis. To detect endogenous MOZART1, 16% tricine SDS gel was used (antibody against MOZART1). Anti-GFP antibody was used to detect EGFP-CEP215^{CM1} and EGFP. The numbers under the membranes represent the relative abundance of γ-tubulin and MOZART1. Related to Fig. 7, D–G. Ctl, control; mAU, milli-absorbance unit.

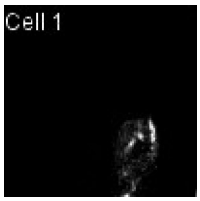

Video 1. **Live cell imaging of Δ/Tetp-*CaMZT1 CaTUB1-GFP* cells without Dox.** Related to Fig. 1 C and Fig. S1 F.

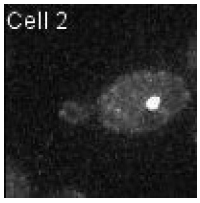

Video 2. **Live cell imaging of Δ/Tetp-*CaMZT1 CaTUB1-GFP* cells with Dox.** Related to Fig. 1 C and Fig. S1 F.

Table S1. **Summary of putative ORF names of γ-TuSC components, γ-TuCRs, and MZT1 in selected fungal species**

Species	SPC97	SPC98	SPC72/Mto1	SPC110/Pcp1	MZT1
Saccharomyces cerevisiae	YHR172W	YNL126W	YAL047C	YDR356W	
Candida glabrata	CAGL0I02464g	CAGL0L04136g	CAGL0M12254g	CAGL0A02596g	
Naumovozyma castellii	NCAS0D01330	NCAS0G02430	NCAS0A07500	NCAS0F03220	
Zygosaccharomyces rouxii	ZYRO0C11792g	ZYRO0G06358g	ZYRO0C00814g	ZYRO0F09570g	
Kluyveromyces lactis	KLLA0A09141g	KLLA0F24222g	KLLA0A03509g	KLLA0E21517g	
Lachancea waltii	Kwal_23.4386	Kwal_YGOB_33.14727	Kwal_26.6821	Kwal_55.21515	
Candida albicans	orf19.708	orf19.2600	orf19.6583	orf19.3100	orf19.4418.1
Candida dubliniensis	CD36_32280	CD36_26890	CD36_71290	CD36_46550	cdub_CGOB_00068
Candida tropicalis	CTRG_00669	CTRG_00880	CTRG_05105	CTRG_03504	ctro_CGOB_00194
Candida parapsilosis	CPAR2_204760	CPAR2_801080	CPAR2_805620	CPAR2_700060	CPAR2_501415
Candida orthopsilosis	CORT0D04870	CORT0A01130	CORT0H01880	CORT0G00170	CORT0B01560
Lodderomyces elongisporus	LELG_03225	LELG_00120	LELG_05026	LELG_03678	
Debaryomyces hansenii	DEHA2G23540g	DEHA2B05500g	DEHA2F09746g	DEHA2G12936g	DEHA2D12298g
Pichia stipitis	PICST_54133	PICST_60226	PICST_68156	psti_CGOB_00003	psti_CGOB_00211
Candida tenuis	CANTEDRAFT_95247	CANTEDRAFT_123515	CANTEDRAFT_113713 (fragment)	CANTEDRAFT_125110 (fragment)	CANTEDRAFT_105081 (wrong start codon)
Spathaspora passalidarum	SPAPADRAFT_54312	SPAPADRAFT_149322	SPAPADRAFT_68792	SPAPADRAFT_48750	spas_CGOB_00034
Pichia guilliermondii	PGUG_04078	PGUG_00818	PGUG_05745	PGUG_04339	(gap)
Clavispora lusitaniae	CLUG_02476	CLUG_03672	CLUG_01471	CLUG_02991	clus_CGOB_00052
Hansenula polymorpha	OPOL_76307	OPOL_91909	OPOL_91673	uniparc/UPI0003DF2AFF	
Pichia pastoris	PAS_chr2-1_0377	PAS_chr2-2_0354	PAS_chr3_0700	PAS_chr4_0295	
Yarrowia lipolytica	YALI0E02816p	YALI0C09757		YALI0A05203	
Neurospora crassa	XP_962067	XP_960965	XP_011395372	XP_959539	(Unannotated, immediately upstream of locus NCU11158.7)
Aspergillus nidulans	CBF70665	CBF76591	CBF82712	CBF83478	XP_658965
Schizosaccharomyces pombe	NP_596044	BAA94097	CAA22653	CAB03608	CCD31316

Table S2. **Summary of plasmids used in this study**

Baculovirus insect cell expression	Plasmid
pTC186-1	pFastBac1-*CaMZT1-3Flag*
pTC193	pFastBac1-*CaTUB4*
pTC194-2	pFastBac-HTA-*CaSPC97*
pTC187	pFastBac-HTA-*CaSPC98*
pTC171-1	pFastBac-HTA-*ScSPC98*$^{CaSPC98\text{-}N}$
pTC321	pFastBac-HTA-*CaSPC98*$^{ScSPC98\text{-}N}$
pTC362-1	pFastBac-HTA-N-Δ*CaSpc98*
pTC176-1	pFastBac-M30a-*CaSPC110-N*
pTC337	pFastBac-M30a-*CaSPC72-N*
E. coli overexpression	
pTC170-1	pET28b-*CaMZT1*
pTC174-1	pET28b-*EGFP-CaMZT1*
pTC385-1	pET28b-*CaMZT1-EGFP*
pTC312-1	pET28b-*CaMZT1-D22A*
pTC313-1	pET28b-*EGFP-CaMZT1-D22A*
pTC167-1	pGEX-6p-1-*CaSPC110-N*
pTC373-1	pGEX-6p-1-*CaSPC110-N-Y137A*
pTC328-1	pGEX-6p-1-*CaSPC110-N-5E*
pTC329-1	pGEX-6p-1-*CaSPC110-N-6E*
pTC350	pGEX-6p-1-*CaSPC110-N-4A*
pTC374	pGEX-6p-1-*CaSPC110-N-9A2*
pTC368-1	pGEX-6p-1-*CaSPC110-N-9A1*
pTC369-3	pGEX-6p-1-*CaSPC110-CM1*
pTC336	pGEX-6p-1-*CaSPC72-N*
pTC355-2	pGEX-6p1-*CaSPC72-N-3A*
pTC372-1	pGEX-6p-1-*CaSPC72N-9A*
pTC353-1	pGEX-6p-1-*CaMZT1*
pTC360-1	pGEX-6p-1-*CaMZT1-D22A*
pTC106 (TK)	pGEX-6p-1-*CEP215-N*
pTC351	pGEX-6p-1-*CEP215-N-F75A*
pTC382-1	pGEX-6p-1-*CEP215-CM1*
pTC069 (TK)	pET28c-*EGFP-MOZART1*
pTC385-1	pET28b-*MOZART1-EGFP*
Human cell transfection	
pTC387-1	pCMV-*HA-hMZT1-EGFP*
C. albicans strain constructions	
pFA-GFP-ARG4	
pFA-NAT1	
pFA-URA3	
pCAU98	
S. cerevisiae strain constructions	
pTC185-1	pRS414-*ScSPC110*$^{CaSPC110\text{-}N}$
pTC169	pRS426-*GAL1p-EGFP-CaMZT1*
pTC184-1	pRS315-*ScSPC98*$^{CaSPC98\text{-}N}$

Table S3. **Summary of *C. albicans* and *S. cerevisiae* strains used in this study**

Strains	Description
C. albicans	
BWP17	*ura3::imm434/ura3::imm434 his1::hisG/his1::hisG arg4::hisG/arg4::hisG*
PY173	*ade2::hisG/ade2::hisG ura3::imm434/ura3::imm434 his1::hisG/his1::hisG arg4::hisG/arg4::hisG ENO1/eno1::ENO1-tetRScHAP4AD-3xHA-ADE2*
LCA009-1	Same as PY173 with *mzt1Δ::URA3/MZT1*
LCA012	Same as PY173 with *MZT1-GFP-ARG4/MZT1*
LCA015-1	Same as PY173 with *MZT1/mzt1::URA3pTet$_{off}$MZT1*
LCA016-1	Same as BWP71 with *mzt1Δ*::SAT1/MZT1
LCA006-1	Same as PY173 with *mzt1Δ*::SAT1/MZT1
LCA001-2	Same as PY173 with *mzt1Δ::SAT1/mzt1::URA3pTet$_{off}$MZT1*
LCA002	Same as PY173 with *mzt1Δ::SAT1/mzt1::URA3pTet$_{off}$MZT1-GFP-ARG4*
LCA010-1	Same as LCA001-2 with *CaSPC97/CaSPC97-GFP-ARG4*
LCA011	Same as LCA001-2 with *CaSPC98/CaSPC98-GFP-ARG4*
LCA004-1	Same as LCA001-2 with *CaTUB1/CaTUB1-GFP-ARG4*
S. cerevisiae	
ESM335-1	*MATa ura3-52 lys2-801 ade2-101 trp1Δ63 his3Δ200 leu2Δ1 spc110Δ::HIS3* pRS316-*ScSPC110*
TCL629-1	*MATa ura3-52 lys2-801 ade2-101 trp1Δ63 his3Δ200 leu2Δ1 spc110Δ::HIS3* pRS316-*SPC110* pRS414-*ScSPC110$^{CaSPC110\text{-}N}$*
ESM243-5	*MATa ura3-52 lys2-801 ade2-101 trp1Δ63 his3Δ200 leu2Δ1 Δspc98::HIS3* pRS316-*ScSPC98*
TLC623-1	*MATa ura3-52 lys2-801 ade2-101 trp1Δ63 his3Δ200 leu2Δ1 Δspc98::HIS3* pRS315-*ScSPC98$^{CaSPC98\text{-}N}$*
TCL638-1	*MATa ura3-52 lys2-801 ade2-101 trp1Δ63 his3Δ200 leu2Δ1 Δspc98::HIS3* pRS315-*ScSPC98* pRS414-*ScSPC110 SPC42-mCherry-hphNT1* pRS316-*GAL1p-EGFP-CaMZT1*
TCL637-1	*MATa ura3-52 lys2-801 ade2-101 trp1Δ63 his3Δ200 leu2Δ1 Δspc98::HIS3* pRS315-*ScSPC98 pRS414-ScSPC110$^{CaSPC110\text{-}N}$ SPC42-mCherry-hphNT1* pRS316-*GAL1p-EGFP-CaMZT1*
TCL634-1	*MATa ura3-52 lys2-801 ade2-101 trp1Δ63 his3Δ200 leu2Δ1 Δspc98::HIS3* pRS315-*ScSPC98$^{CaSPC98\text{-}N}$* pRS414-*ScSPC110 SPC42-mCherry-hphNT1* pRS316-*GAL1p-EGFP-CaMZT1*
TCL636-1	*MATa ura3-52 lys2-801 ade2-101 trp1Δ63 his3Δ200 leu2Δ1 Δspc98::HIS3* pRS315-*ScSPC98$^{CaSPC98\text{-}N}$* pRS414-*ScSPC110$^{CaSPC110\text{-}N}$ SPC42-mCherry-hphNT1* pRS316-*GAL1p-EGFP-CaMZT1*

Reference

Hanson, S.J., K.P. Byrne, and K.H. Wolfe. 2014. Mating-type switching by chromosomal inversion in methylotrophic yeasts suggests an origin for the three-locus *Saccharomyces cerevisia*e system. *Proc. Natl. Acad. Sci. USA*. 111:E4851–E4858. http://dx.doi.org/10.1073/pnas.1416014111